Optimal selection of proton exchange membrane fuel cell condition monitoring thresholds

Pavle Boškoski[a,*], Andrej Debenjak[a,b]

[a]*Jožef Stefan Institute, Department of Systems and Control, Jamova cesta 39, SI-1000 Ljubljana, Slovenia*
[b]*Jožef Stefan International Postgraduate School, Jamova cesta 39, SI-1000 Ljubljana, Slovenia*

Abstract

When commissioning or restarting a system after a maintenance action there is a need to properly tune the decision thresholds of the diagnostic system. Too low or too high thresholds may implicate either missed alarms or false alarm rates. This paper suggest an efficient data-driven approach to optimal setting of decision thresholds for a PEM fuel cell system based solely on data acquired from the system in reference state of health (i.e. under fault free operation). The only design parameter is the desired false alarm rate. Technically, the problem reduces to analytically determining the probability distribution of the fuel cell's complex impedance and its particular components. Employing pseudo-random binary sequence perturbation signals, the distribution of the impedance is estimated through the complex wavelet coefficients of the fuel cell voltage and current. The approach is validated on a PEM fuel cell system subjected to various faults.

Keywords: PEM fuel cell system, Fault detection, Complex random variable, Probability of false alarm

1. Introduction

Like any other item of equipment the reliability and durability of proton exchange membrane (PEM) fuel cells is affected by faults on various components [1, 2]. These faults include corrosion of the electrodes and degradation of membranes [3–6], catalyst and membrane poisoning [7–10], and water management faults (i.e. flooding of gas channels and membrane drying) [11–13]. Timely detection and diagnosis of these faults is of great importance for future employment of PEM fuel cell technology on larger scale [14, 15].

Majority of faults that may occur on PEM fuel cells can be detected with multitude of approaches based on electrochemical impedance spectroscopy (EIS) [16–21]. EIS characterization of fuel cell flooding and membrane drying was reported by plethora of authors [22–28]. Portion of these authors used EIS measurement data to directly detect faults [26–28], meanwhile others proposed model based approaches [22–25]. Employing somehow more advanced approach, Kadyk et al. [29, 30] proposed a non-linear extension of the EIS diagnostic approach with non-linear frequency response

analysis (NFRA) to diagnose fuel cell flooding and membrane dehydration. In addition to the detection of water management faults, Le Canut et al. [27] and Kadyk et al. [31] also tackled detection of anode catalyst poisoning with CO by employing more complex NFRA. All these numerous studies confirm that various PEM fuel cell faults can be observed through EIS impedance measurements. Therefore, an autonomous and effectual condition monitoring system for fuel cells can be implemented by using EIS features.

To the best of the authors' knowledge, at this stage of PEM fuel cell diagnostic's development, using EIS features for condition monitoring requires beforehand EIS characterisation of fuel cell behaviour under normal and faulty operation. Having such data, one can set up threshold values that mark the border between fault free and faulty regions.

However, performing such characterisation procedures may be infeasible in many practical situations, since they may lead to irreversible damage of the fuel cell system (e.g. extensive drying and CO poisoning [1, 2]). Moreover, due to variation in parameters from one fuel cell to another, once the EIS data is obtained for one particular fuel cell, there is no straightforward way to transfer this particular knowledge to another cell without conducting new complete set of char-

---

*Corresponding author.
Email address: `pavle.boskoski@ijs.si` (Pavle Boškoski)

acterisation procedure. Therefore a vital question arises how to design a condition monitoring system employing measurements conducted solely under fault free (normal) operation of a fuel cell.

Implementing an effective condition monitoring system can significantly improve the operation of in-the-field fuel cell power units [32]. Many of the problems for designing an effective condition monitoring system have been addressed in the context of mechanical systems [33, 34]. The main difficulty is to determine the statistical properties of the selected features and model their behaviour under faulty conditions [35, 36]. Achieving this goal has significant practical importance for any system integrator.

Addressing the issue of beforehand characterisation, this paper proposes a systematic approach for determining the bounds of the fault free region of operation without inducing any faults. In the proposed approach the fuel cell impedance is considered as a complex random variable. The corresponding probability distribution functions are derived, allowing complete statistical characterisation of the behaviour of the complex impedance. As a result, the only design parameter is the desired false alarm rate, which is intuitive and very well understood even by non-specialists in the area of condition monitoring. The effectiveness of the proposed approach was evaluated on a 8.5 kW PEM fuel cell subjected to various water management faults.

The first step towards specifying the fault free region is the analysis of the statistical properties of the feature set as described in Section 2. Using these statistical properties the method for calculating the bounds of the fault free region as well as the overall condition indicator are presented in Section 3. Experimental evaluation of the proposed condition indicator is presented in Section 4.

2. Statistical properties of the fuel cell impedance

Fuel cell electrical impedance is a complex variable that is defined as a frequency domain ratio of the voltage to the current. Regarding the fuel cell system as linear and time invariant one, the electrical impedance can be referred as its transfer function which has a deterministic nature for each frequency. However, when dealing with real world scenarios the observed fuel cell system is influenced by external disturbances, which are generally modelled as stochastic signals [37], as shown in Figure 1. Since these disturbances are in many cases unmeasurable, their influence is incorporated into the model thus making the mapping between the current and voltage a stochastic one. Therefore, the observed

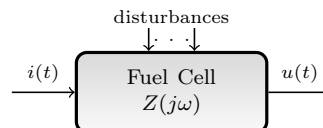electrical impedance should be treated as a complex random variable.

Figure 1: Representation of fuel cell system excited by current and affected by disturbances

In order to properly describe the electrical impedance as a complex random variable, the first step is determining its probability distribution function. For that purpose the fuel cell system can be excited using pseudo-random binary sequence (PRBS) signal [38]. Following the procedure described by Debenjak et al. [38], the impedance characteristic can be efficiently estimated by using the complex wavelet coefficients of the continuous wavelet transform of the fuel cell's current $i(t)$ and voltage $u(t)$ using the Morlet mother wavelet, which is used in a variety of fields [38–41].

2.1. Continuous wavelet transform using the Morlet wavelet

The continuous wavelet transform (CWT) of a square integrable function $f(t) \in \mathbf{L}^2(\mathbb{R})$ is defined as [42]:

$$Wf(s,u) = \langle f(t), \psi_{u,s}(t) \rangle = \int_{-\infty}^{\infty} f(t)\psi_{u,s}^*(t)\,dt, \quad (1)$$

where $\psi_{u,s}(t)$ is a scaled and translated version of the mother wavelet $\psi(t)$:

$$\psi_{u,s}(t) = \frac{1}{\sqrt{s}}\psi\left(\frac{t-u}{s}\right). \quad (2)$$

The wavelet coefficients (1) describe the analysed signal $f(t)$ on the time-scale plane. The conversion between scale s and frequency f is straightforward and depends on the selection of the mother wavelet (2). Therefore, in the remaining of the paper instead of scale s all subsequent relations will rely on actual frequency f.

For the impedance estimation, one needs information about the instantaneous amplitude and phase of the electrical current $i(t)$ and voltage $u(t)$. Therefore, the Morlet wavelet was chosen as a mother wavelet (2), which reads [43]:

$$\psi(t) = \pi^{-1/4}\left(e^{j\omega_0 t} - e^{-\omega_0^2/2}\right)e^{-t^2/2}, \quad (3)$$

where ω_0 is the ratio between the highest and the second most highest peak and is usually set to $\omega_0 = 5$.

The Morlet wavelet (3) is an analytical function i.e. it has only positive frequencies. As a result, the wavelet coefficients $Wf(t, f)$ in (1) are complex values and at each time translation t and frequency f the wavelet coefficients give the instantaneous amplitude and phase.

2.2. PRBS as excitation signal

PRBS can be regarded as sufficiently close to stationary random noise whose amplitude probability distribution is Gaussian [44]. Analysing such a signal with continuous wavelet transform preserves its statistical properties with in the wavelet coefficients. As a result the complex wavelet coefficients of the measured current $i(t)$ and voltage $u(t)$ for a particular frequency can be regarded as zero-mean Gaussian circular complex random variables:

$$Wi(t, f) = \Re\{Wi(t, f)\} + j\Im\{Wi(t, f)\}$$
$$Wu(t, f) = \Re\{Wu(t, f)\} + j\Im\{Wu(t, f)\}, \quad (4)$$

where $Wi(t, f)$ and $Wu(t, f)$ are the complex wavelet coefficients of the current $i(t)$ and voltage $u(t)$ respectively. Basic definitions about complex circular random variables are given in the Appendix B.

Due to the circularity of the complex random variables as well as the statistical properties of the PRBS signal, the complex wavelet coefficients have the following properties:

$$\Re\{Wi(t, f)\}, \Im\{Wi(t, f)\} \sim \mathcal{N}(0, \sigma_i^2)$$
$$\Re\{Wu(t, f)\}, \Im\{Wu(t, f)\} \sim \mathcal{N}(0, \sigma_u^2). \quad (5)$$

Using the complex wavelet coefficients (5), the impedance at particular frequency $f = f_0$ can be calculated as a ratio of the complex wavelet coefficients as:

$$z(t) = \left.\frac{Wu(t, f)}{Wi(t, f)}\right|_{f=f_0} = z_r + jz_i. \quad (6)$$

2.3. Probability distribution of the complex impedance $z(t)$

The ratio of two independent circular Gaussian complex random variables is a known result [45]. However, the current $i(t)$ and voltage $u(t)$ are correlated. This correlation can be expressed with the covariance matrix

$$\Sigma = \begin{bmatrix} \sigma_u^2 & \rho\sigma_u\sigma_i \\ \rho^*\sigma_u\sigma_i & \sigma_i^2 \end{bmatrix}, \quad (7)$$

where $\rho = \rho_r + j\rho_i$ is complex correlation coefficient, such as $|\rho| \le 1$. As a result the distribution of the ratio (6) reads [46]:

$$f_z(z) = \frac{1 - |\rho|^2}{\pi\sigma_u^2\sigma_i^2}\left(\frac{|z|^2}{\sigma_u^2} + \frac{1}{\sigma_i^2} - 2\frac{\rho_r z_r - \rho_i z_i}{\sigma_u\sigma_i}\right)^{-2}, \quad (8)$$

The location of the mode of $f_z(z)$ depends on the correlation coefficient ρ. For $\rho = 1/2 + j1/4$ the shape of (8) is shown in Figure 2.

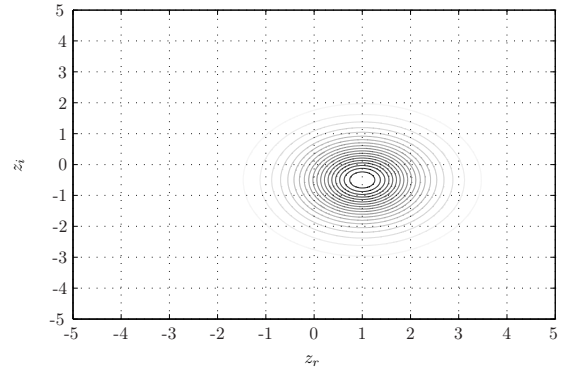

Figure 2: Contour plot of the probability density function (8) for $\rho = 1/2 + j1/4$

2.4. Probability distribution functions of the real z_r and imaginary z_i impedance components

The distribution of the real z_r and imaginary z_i components of the impedance (6) can be derived from the distribution (8). The probability distribution functions of the imaginary component z_i reads [46]:

$$f_{z_i}(z_i|\rho_r, \rho_i) = \frac{\left(1 - |\rho|^2\right)\sigma_x^2\sigma_y}{2\left((1 - \rho_r^2)\sigma_x^2 + 2z_i\rho_i\sigma_x\sigma_y + z_i^2\sigma_y^2\right)^{3/2}} \quad (9)$$

For the real component z_r the probability distribution function has the same shape and reads:

$$f_{z_r}(z_r|\rho_r, \rho_i) = f_{z_i}(z_r| - \rho_i, -\rho_r). \quad (10)$$

The shape of the (9) and (10) are shown in Figures 3(a) and 3(b).

2.5. Probability distribution function of the impedance amplitude $|z(t)|$

Besides the probability distribution of the real z_r and imaginary z_r components of the impedance in many cases the module of the complex impedance can be used as a feature in the process of condition monitoring. For the circular Gaussian complex random variables (5), their corresponding modules $|Wu(t, f_0)|$ and $|Wi(t, f_0)|$ are distributed with Rayleigh distribution as:

$$|Wu(t, f_0)| \sim \text{Rayleigh}(\sigma_u)$$
$$|Wi(t, f_0)| \sim \text{Rayleigh}(\sigma_i). \quad (11)$$

(a) Distribution of $\Re(Z)$

(b) Distribution of $\Im(Z)$

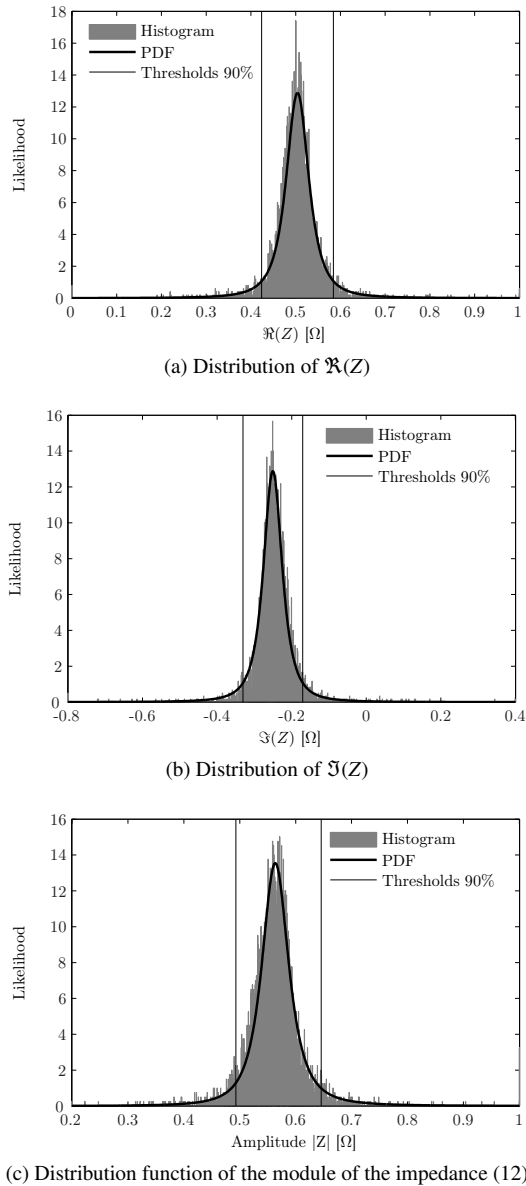(c) Distribution function of the module of the impedance (12)

Figure 3: Probability distribution functions of particular impedance components

As the current $i(t)$ and voltage $u(t)$ are correlated, the probability distribution function of the module of the ratio (6) reads [47]:

$$p_{|Z|}(|z|) = \frac{2\sigma_i^2 \sigma_u^2 (1 - \rho^2)|z|(\sigma_i^2|z| + \sigma_u^2)}{\left[(\sigma_i^2|z|^2 + \sigma_u^2)^2 - 4\rho^2 \sigma_u^2 \sigma_i^2 |z|^2\right]^{3/2}}, |z| \geq 0,$$
(12)

where $|\rho| \leq 1$ is the correlation coefficient, as defined in (7). The probability distribution function (12) is positively skewed and defined on the non-negative semi axis. A typical realisation of the probability distribution function (12) is shown in Figure 3(c).

2.6. Parameter estimation

The probability distribution functions (8), (9) and (12) depend on three parameters σ_u, σ_i and the correlation coefficient ρ. These parameters can be easily estimated through the covariance matrix (7) by using the calculated wavelet coefficients as:

$$E\{Wu(t, f_0)Wu(t, f_0)^*\} = \frac{\sigma_u^2}{2}$$

$$E\{Wi(t, f_0)Wi(t, f_0)^*\} = \frac{\sigma_i^2}{2} \qquad (13)$$

$$E\{Wi(t, f_0)Wu(t, f_0)^*\} = \frac{\sigma_u \sigma_i}{2}\rho.$$

The histogram of the impedance components and its module, using a single realisation of the complex wavelet coefficients (5), are shown in Figure 3. Using the estimated parameters σ_u, σ_i and ρ, the corresponding probability distribution functions clearly correspond to the empirically estimated histograms.

3. Fuel cell condition indicator based on the probability of false alarm

The statistical properties of the complex impedance are completely determined by estimating the parameters (13) using the data from the fault free operation. Deciding whether the fuel cell's condition deteriorated can be performed by calculating the probability of observing a particular impedance value. Determining the optimal values at which the deterioration can be regarded as significant is of great importance for an autonomous condition monitoring system. The most commonly used criterion for determining these boundary values selection is low probability of false alarm (PFA) [35].

Condition monitoring system based on low PFA will raise alarms only when the condition of the fuel cell is suboptimal. Having derived the probability distribution functions (9) and (12), determining optimal boundary values based on low PFA is straight forward and can be defined as:

$$T = 1 - F^{-1}(PFA) = 1 - \inf\{F(z) \geq PFA\}, \qquad (14)$$

where $F(z)$ is the cumulative distribution function of either (9) or (12)[1] and z is the corresponding impedance component. This approach was used for calculating the thresholds values in Figure 3 for $PFA=10\%$.

---

[1]Corresponding cumulative distribution functions are derived in the Appendix A.

3.1. Condition indicator

Selected threshold values (14) can be additionally used for mapping the complex impedance values into an so-called condition indicator (CI). It is an abstract feature defined on the interval $[0, \infty)$ that can be directly related to the condition of the system [35]. For a healthy system CI should acquire low values, typically $CI = 0$. As the condition deteriorates, the value of CI should increase in accordance with the severity of the fault(s) present in the system. Using PFA value, the value of CI are typically scaled in such a way that values close to one should indicate imminent failure. Having such a feature value with fixed threshold determining imminent failure has two major advantages:

1. it gives an unified and scale-free view of the overall system condition and

2. its trend can be used for prognostics i.e. estimation of the remaining useful life.

In the context of fuel cells, the presence of fault can either increase or decrease certain impedance components. Therefore, for fault free operation the value of the CI will be in the middle of the region bounded by thresholds at certain PFA, as shown in Figure 3.

The mapping into the corresponding CI can be easily achieved by using the cumulative distribution functions of either (9) or (12) for the corresponding impedance components. As a result the impedance components of the fault free region will acquire values in the vicinity of $^1\!/\!_2$. Setting the maximal value for the CI to be the chosen PFA, the final scaling relation reads:

$$CI = 2 \times (1 - PFA)^{-1} \left| F(z) - \frac{1}{2} \right|, \qquad (15)$$

where $F(z)$ is the cumulative distribution function of the corresponding impedance component, as derived in the Appendix A.

4. Experimental evaluation

4.1. Experimental setup

The test bed incorporated a PEM fuel cell power unit, electronic load, arbitrary function generator, voltage and current measurement equipment, and desktop computer. The measurements were performed on a commercially available PEM fuel cell system HyPM HD 8 produced by Hydrogenics Corporation. The stack consists of 80 PEM fuel cells each with surface area of 200 cm^2, providing 8.5 kW of electric power in total. The fuel cell system operates on pure hydrogen and ambient air.

The electronic load was used to simulate real electrical load and to perturb the fuel cell system with PRBS perturbation signal in galvanostatic mode. The e-load's current was controlled by an arbitrary function generator, which was generating the PRBS reference signal. Block diagram of the experimental setup is presented in Figure 4.
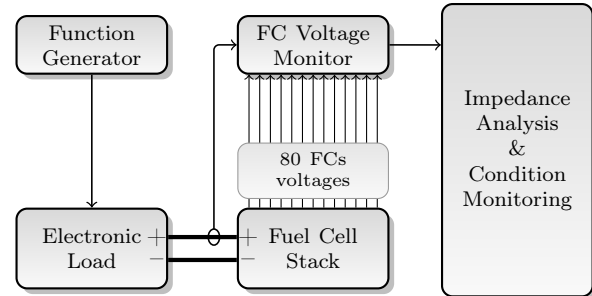

Figure 4: Block diagram of the experimental setup.

Voltage and current signals were measured with an in-house developed fuel cell voltage monitor (FCVM) presented in Figure 5 [23]. The top view of the Figure 5 shows the printed circuit board of the FCVM. The board is mounted directly on top of the stack and the galvanic contacts to all the fuel cells are implemented by spring contact probes, which are visible in the side view of the Figure 5. The FCVM provides the means for fast and accurate measurements of voltage and current signals of any individual fuel cell inside the stack (the contacts to all fuel cells of the stack are clearly seen at the bottom edge of Figure 5). The FCVM utilizes a Hall-effect current sensor to measure current, and an analogue circuitry to precisely measure changes in voltage of any individual fuel cell inside the stack.

The FCVM enables measurement of voltage and current signals with the resolution of 80 μV and 10 mA, respectively, at sampling frequency of 5 kHz. It has a frequency range of up to 660 Hz. The FCVM contains a CAN bus interface for data transmission to external device (e.g. personal computer). Signal processing and computational algorithms were performed on a PC.

4.2. Experimental procedure

During the experiments, the fuel cell system was kept at constant operating and environmental conditions. The fuel cell stack temperature and the stoichiometry were kept constant by the built-in controller supplied by the fuel cell manufacturer Hydrogenics at 50°C and 2.5, respectively. At the cathode side, the temperature and relative humidity of the inlet air were measured with Vaisala HMP235A transducer and controlled
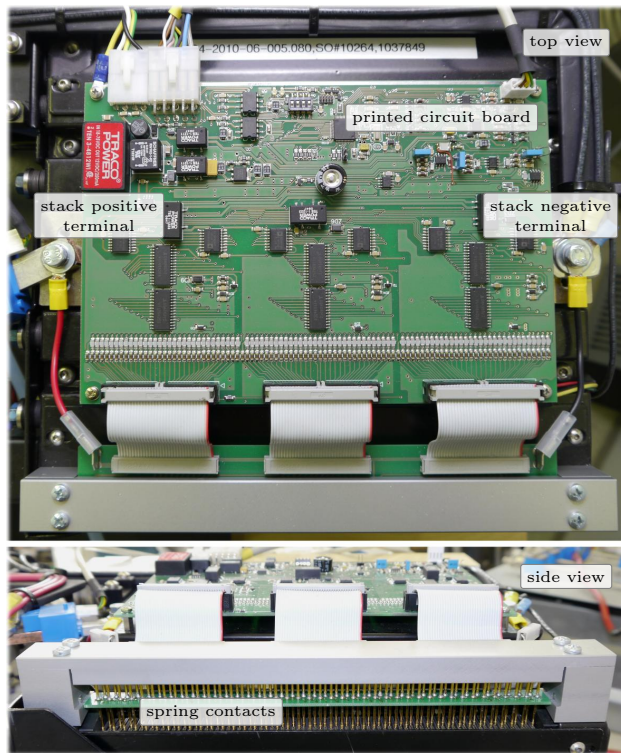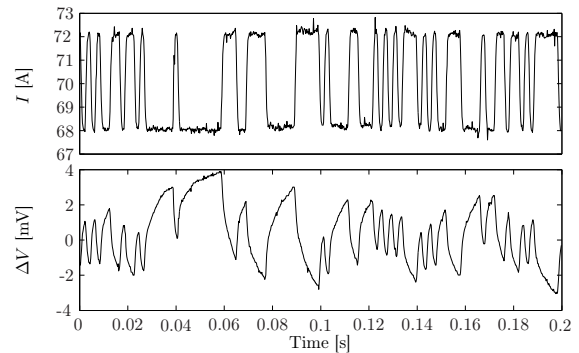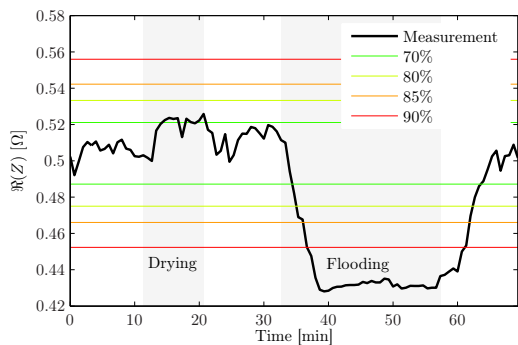
Figure 6: Measured current and voltage signals during the experiment.

the fuel cell was slightly dried down to relative humidity of 5% (4.1 g/m^3) for about 10 minutes, between the 12th and the 22nd minute, in order to induce membrane drying, and again humidified to 9%. Afterwards, between the 34th and the 58th minute, saturated air with relative humidity of 100% (83 g/m^3), was fed into the fuel cell system inducing flooding of fuel cells. Finally, the air humidity was decreased down to the initial 9%. Using such a cycle we were able to determine the response of the cell under different fault scenarios with various fault severity. These stages of the experiment are clearly indicated in Figure 7.
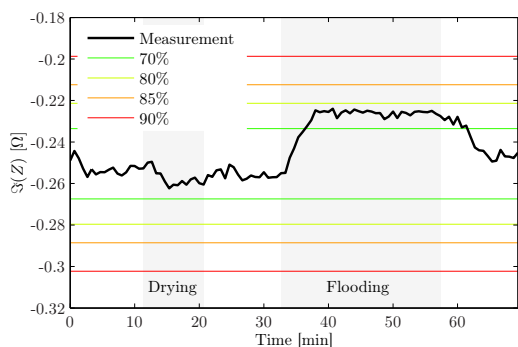
4.3. Time evolution of particular impedance components

Using the complex wavelet coefficients (4), calculated from the initial fault free operation signals, the parameters of probability distribution functions (8) and (12) were estimated employing (13). With the estimated parameters, the threshold values were calculated for four different $PFA = \{25\%, 20\%, 15\%, 10\%\}$. The resulting thresholds for each impedance component are shown in Figure 7. The threshold values clearly define the fault free region.
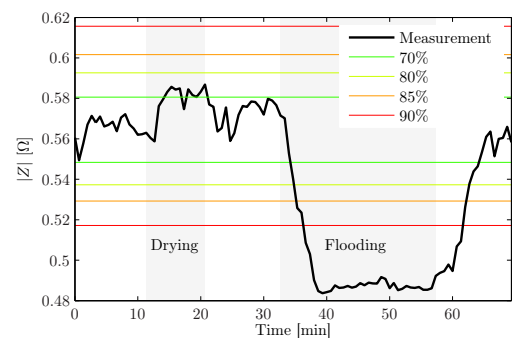
The first departure from the fault free condition was between the 12th and the 22nd minute, when the fuel cell was fed with somewhat drier air (5% relative humidity). In that particular region the real component of the impedance increased and surpasses the threshold of 70%, as shown in Figures 7(a) and 7(b). Similar observation can be made also for the module of the impedance, as shown in Figure 7(c). Despite the minute changes in the relative humidity of the inflow air, there are clear change in the value of the impedance, with 30% probability of false alarm. Without the threshold

Figure 5: Top and side view of the FCVM connected to a 8.5 kW PEM fuel cell system.

by external PID controllers. The temperature of the air flow was kept constant at 50°C and the relative humidity changed in order to introduce drying or flooding accordingly. At the anode side, the fuel cell was fed with pure and dry hydrogen at constant temperature of 20°C. The DC current operating point I_{dc} was set to 70 A resulting in the stack voltage of 55 V, whereas the amplitude of the superposed PRBS waveform was set to 2 A. As such, the peak-to-peak amplitude was 4 A and therefore small enough not to cause difficulties due to non-linearity of the PEM fuel cells. Figure 6 shows time plots of current and voltage signals of a PEM fuel cell during measurements. Current was measured as an absolute value, whereas the fuel cell voltage was measured as differential value.

During the experiment, an acquisition of measurements occurred every 40 seconds. The experiment went through five stages. In the first stage of approx. 11 minutes, 18 measurements were performed in the fault free state at which the relative humidity of the inlet air was kept at 9% (which at 50°C corresponds to 7.5 g/m^3 - grams of water per cubic meter of air). Then, air fed to

(a) Values of $\Re(Z)$

(b) Values of $\Im(Z)$

(c) Values of $|Z|$

Figure 7: Trend of impedance components throughout the experiment

values such a quantification would have been impossible.

Unlike the minor changes caused by the mild decrease in the humidity, the flooding with 100% saturated air inflow shows significant changes in al three impedance components. The values of $\Re(z)$ and $|z|$, between the 34th and the 58th minute, indicate that the condition of the fuel cell departed from the fault free area, with less then 10% probability of false alarm, as shown in Figures 7(a) and 7(c). The change in the imaginary

component $\Im(z)$ is somewhat smaller, the probability of false alarm is less then 30%.

Finally, when the relative humidity of the air inflow was returned to normal the impedance components returned to the initial values within the fault free region.

4.4. Time evolution of the CI

The time evolution of the CI (15) of the impedance module $|z|$ is shown in Figure 8. The values of the CI were calculated using the mapping relation (15) with $PFA = 90\%$.
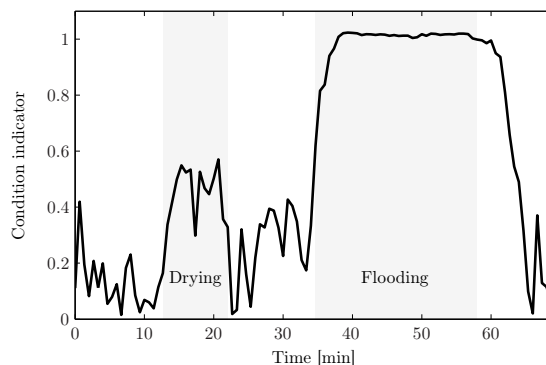

Figure 8: Trend of CI of $|Z|$ throughout the experiment

By analysing this time evolution one can notice that during the fault free operation CI acquires low values. As the first fault was induced, the values of CI increased up to 0.5, which indicates that the condition of the fuel cell deteriorated. The acquired value of 0.5 clearly shows departure from fault free operation while in the same time is inline with the low severity of the induced drying, relative humidity change of 8%. Unlike the low severity of the drying fault, during the flooding phase of the experiment, the value of CI surpasses the limit value of 1. The overwhelming flooding of the system is directly reflected in the high value of the CI. Finally, at the end of the experiment, when the air condition was back to nominal, the values of CI decreased indicating almost fault free operation.

The results confirm the behaviour of CI. It is sufficiently sensitive on deviation in the condition of the water management. In the same time its value is directly related to the severity of the deviation with respect to the selected PFA.

5. Conclusion

Observing the impedance of a fuel cell in the context of random variables, this paper specifies probability

distribution functions of the real and imaginary components as well as its module. Using the data solely from the fault free operation, one can estimate the free parameters of these distribution functions. As a result, threshold values defining the fault free region can be calculated by specifying a specific probability of false alarm.

Determining the threshold values using the probability of false alarm has significant practical merit. For each of the measured impedance components one can calculate the probability of false alarm and use this value as an indicator of confidence that the current condition of the fuel cell has sufficiently departed from the fault free region. Furthermore, the proposed condition indicator scaled with the chosen PFA is directly related to the fault severity and can be used for both fault detection as well as estimation of the remaining useful life. The evaluation of the proposed method confirms that the calculated condition indicator based on the PFA corresponds to the severity of the induced faults.

Acknowledgment

Appendix A. Cumulative distribution functions

Appendix A.1. Cumulative distribution function of z_i

According to Baxley et al. [46] integrating out z_r from (8) results into the following cumulative distribution function:

$$F_{z_i}(z_i|\rho_r, \rho_r) = \frac{1}{2} + \frac{\rho_i \sigma_u + z_i \sigma_i}{2\sqrt{(1 - \rho_r^2)\sigma_u^2 + 2z_i\rho_i\sigma_u\sigma_i + z_i^2\sigma_i^2}} \tag{A.1}$$

Solution of (A.1) for arbitrary $y = PFA$ reads:

$$z_i = \frac{-2(y - 1)y\rho_i\sigma_u\sigma_i}{2(-1 + y)y\sigma_i^2}$$
$$\pm \frac{\sqrt{(1 - 2y)^2(y - 1)y(|\rho|^2 - 1)\sigma_u^2\sigma_i^2}}{2(-1 + y)y\sigma_i^2} \tag{A.2}$$

Appendix A.2. Cumulative distribution function of $|z|$

The cumulative distribution function that corresponds to (12) reads [47]:

$$F_{|z|}(z) = \frac{1}{2} - \frac{\sigma_u^2 - z^2\sigma_i^2}{2\sqrt{4z^2(1 - \rho^2)\sigma_i^2\sigma_u^2 + (\sigma_u^2 - z^2\sigma_i^2)^2}}, \tag{A.3}$$

where $z \geq 0$. Solution of (A.3) for $y = PFA$ reads:

$$z = \sigma_u \left(\frac{-1 + 2y - 2y^2 + (1 - 2y)^2\rho^2}{2(-1 + y)y\sigma_i^2} \right.$$
$$\left. \pm \frac{(1 - 2y)\sqrt{-1 + \rho^2}\sqrt{(1 - 2y)^2\rho^2 - 1}}{2(-1 + y)y\sigma_i^2} \right)^{1/2} \tag{A.4}$$

Appendix B. Circular complex random variables

A Gaussian complex random variable can analysed through its real and imaginary components

$$Z = X + jY, \tag{B.1}$$

where both X and Y and real Gaussian random variables. In order for the complex Gaussian random variable Z to be circular the following conditions have to be fulfilled [48]:

$$E[Z^2] = E[X^2] - E[Y^2] + jE[XY] = 0. \tag{B.2}$$

As both X and Y are Gaussian random variables in order for (B.2) to be fulfilled

$$E[X^2] = E[Y^2]$$
$$E[XY] = 0. \tag{B.3}$$

Therefore the random variables X and Y are independent with same variance.

Appendix B.1. Circularity of spectral components

A stationary random signal can be represented using Cramer representation [49]:

$$x(t) = \int_{-\infty}^{\infty} e^{j\omega t} dZ(\omega), \tag{B.4}$$

where $dZ(\omega)$ are complex random variables directly related to the signals power spectrum with the following properties:

$$E[dZ(\omega)] = 0, \quad E[dZ(\omega_1)dZ(\omega_2)] = 0, \text{ for } \omega_1 \neq \omega_2. \tag{B.5}$$

Therefore for stationary signals the complex random variables $dZ(\omega)$ are circular [48].

References

[1] F. A. de Bruijn, V. A. T. Dam, G. J. M. Janssen, Fuel Cells 8 (2008) 3–22. doi:10.1002/fuce.200700053.

[2] W. Schmittinger, A. Vahidi, J. Power Sources 180 (2008) 1–14. doi:10.1016/j.jpowsour.2008.01.070.

[3] H. R. Colón-Mercado, B. N. Popov, J. Power Sources 155 (2006) 253–263. doi:10.1016/j.jpowsour.2005.05.011.

[4] R. Borup, J. Meyers, B. Pivovar, Y. S. Kim, R. Mukundan, N. Garland, D. Myers, M. Wilson, F. Garzon, D. Wood, P. Ze-lenay, K. More, K. Stroh, T. Zawodzinski, J. Boncella, J. E. McGrath, M. Inaba, K. Miyatake, M. Hori, K. Ota, Z. Ogumi, S. Miyata, A. Nishikata, Z. Siroma, Y. Uchimoto, K. Yasuda, K.-i. Kimijima, N. Iwashita, Chem. Rev. 107 (2007) 3904–3951. doi:10.1021/cr050182l.

[5] P. T. Yu, Z. Liu, R. Makharia, J. Electrochem. Soc. 160 (2013) F645–F650. doi:10.1149/2.120306jes.

[6] J. D. Fairweather, D. Spernjak, A. Z. Weber, D. Harvey, S. Wes-sel, D. S. Hussey, D. L. Jacobson, K. Artyushkova, R. Mukun-dan, R. L. Borup, J. Electrochem. Soc. 160 (2013) F980–F993. doi:10.1149/2.024309jes.

[7] C. Farrell, C. Gardner, M. Ternan, J. Electrochem. Soc. 171 (2007) 282 – 293. doi:10.1016/j.jpowsour.2007.07.006.

[8] X. Cheng, Z. Shi, N. Glass, L. Zhang, J. Zhang, D. Song, Z.-S. Liu, H. Wang, J. Shen, J. Power Sources 165 (2007) 739 – 756.

[9] W.-M. Yan, H.-S. Chu, M.-X. Lu, F.-B. Weng, G.-B. Jung, C.-Y. Lee, J. Power Sources 188 (2009) 141 – 147. doi:10.1016/j.jpowsour.2008.11.107.

[10] G. Postole, A. Auroux, Int. J. Hydrogen Energy 36 (2011) 6817 – 6825. doi:10.1016/j.ijhydene.2011.03.018.

[11] H. Li, Y. Tang, Z. Wang, Z. Shi, S. Wu, D. Song, J. Zhang, K. Fatih, J. Zhang, H. Wang, Z. Liu, R. Abouatallah, A. Mazza, J. Electrochem. Soc. 178 (2008) 103 – 117. doi:10.1016/j.jpowsour.2007.12.068.

[12] N. Yousfi-Steiner, P. Moçotéguy, D. Candusso, D. Hissel, A. Hernandez, A. Aslanides, J. Power Sources 183 (2008) 260 – 274. doi:10.1016/j.jpowsour.2008.04.037.

[13] T. Ous, C. Arcoumanis, J. Power Sources 240 (2013) 558 – 582. doi:10.1016/j.jpowsour.2013.04.044.

[14] M. Jouin, R. Gouriveau, D. Hissel, M.-C. Péra, N. Zer-houni, Int. J. Hydrogen Energy 38 (2013) 15307 – 15317. doi:10.1016/j.ijhydene.2013.09.051.

[15] M. Jouin, R. Gouriveau, D. Hissel, M.-C. Péra, N. Zer-houni, Int. J. Hydrogen Energy 39 (2014) 481 – 494. doi:10.1016/j.ijhydene.2013.10.054.

[16] J. Stumper, M. Löhr, S. Hamada, J. Power Sources 143 (2005) 150–157. doi:10.1016/j.jpowsour.2004.11.036.

[17] X.-Z. Yuan, H. Wang, J. C. Sun, J. Zhang, Int. J. Hydrogen En-ergy 32 (2007) 4365–4380.

[18] J. Wu, X. Z. Yuan, H. Wang, M. Blanco, J. J. Martin, J. Zhang, Int. J. Hydrogen Energy 33 (2008) 1735–1746. doi:10.1016/j.ijhydene.2008.01.013.

[19] R. Petrone, Z. Zheng, D. Hissel, M. Péra, C. Pianese, M. Sor-rentino, M. Becherif, N. Yousfi-Steiner, Int. J. Hydrogen Energy 38 (2013) 7077–7091. doi:10.1016/j.ijhydene.2013.03.106.

[20] Z. Zheng, R. Petrone, M. Péra, D. Hissel, M. Becherif, C. Pi-anese, N. Y. Steiner, M. Sorrentino, Int. J. Hydrogen Energy 38 (2013) 8914–8926. doi:10.1016/j.ijhydene.2013.04.007.

[21] S. M. Rezaei Niya, M. Hoorfar, J. Power Sources 240 (2013) 281–293. doi:10.1016/j.jpowsour.2013.04.011.

[22] N. Fouquet, C. Doulet, C. Nouillant, G. Dauphin-Tanguy, B. Ould-Bouamama, J. Electrochem. Soc. 159 (2005) 905–913.

[23] A. Debenjak, M. Gašperin, J. Petrovčič, Chem. Eng. Trans. 33 (2013) 1003–1008. doi:10.3303/CET1333168.

[24] S. Cruz-Manzo, R. Chen, J. Electrochem. Soc. 160 (2013) F1109–F1115. doi:10.1149/2.025310jes.

[25] M. Gašperin, , P. Boškoski, A. Debenjak, J. Petrovčič, Fuel Cells (2014) InPress.

[26] W. Merida, D. Harrington, J. L. Canut, G. McLean, J. Power Sources 161 (2006) 264–274. doi:10.1016/j.jpowsour.2006.03.067.

[27] J.-M. Le Canut, R. M. Abouatallah, D. A. Harrington, J. Elec-trochem. Soc. 153 (2006) A857–A864.

[28] A. Debenjak, M. Gašperin, B. Pregelj, M. Atanasijević-Kunc, J. Petrovčič, V. Jovan, J. Mech. Eng. 59 (2013) 56–64. doi:10.5545/sv-jme.2012.640.

[29] T. Kadyk, R. Hanke-Rauschenbach, K. Sund-macher, J. Electroanal. Chem. 630 (2009) 19 – 27. doi:10.1016/j.jelechem.2009.02.001.

[30] T. Kadyk, R. Hanke-Rauschenbach, K. Sundmacher, Int. J. Hydrogen Energy 37 (2012) 7689 – 7701. doi:10.1016/j.ijhydene.2012.01.148, 7th Petite Workshop on the Defect Chemical Nature of Energy Materials, 14-17 March 2011, Storaas, Kongsberg, Norway.

[31] T. Kadyk, R. Hanke-Rauschenbach, K. Sundmacher, J. Appl. Electrochem. 41 (2011) 1021–1032. doi:10.1007/s10800-011-0298-8.

[32] B. Pregelj, D. Vrečko, V. Jovan, J. Power Sources 196 (2011) 9419–9428. doi:10.1016/j.jpowsour.2011.06.077.

[33] G. Vachtsevanos, F. L. Lewis, M. Roemer, A. Hess, B. Wu, Intel-ligent Fault Diagnosis and Prognosis for Engineering Systems, Wiley, 2006.

[34] A. Jardine, D. Lin, D. Banjevič, Mech. Syst. Signal Process. 20 (2006) 1483–1510.

[35] E. Bechhoefer, A. Bernhard, in: IEEE Aerospace Conference, pp. 1–9.

[36] P. Boškoski, Đ. Juričić, Mech. Syst. Signal Process. 31 (2012) 369—381.

[37] R. Isermann, M. Münchhof, Identification of Dynamic Systems: An Introduction with Applications, Advanced textbooks in con-trol and signal processing, Springer-Verlag Berlin Heidelberg, 2011. doi:10.1007/978-3-540-78879-9.

[38] A. Debenjak, P. Boškoski, B. Musizza, J. Petrovčič, Đ. Juričić, J. Power Sources 254 (2014) 112 – 118. doi:10.1016/j.jpowsour.2013.12.094.

[39] B. Musizza, A. Stefanovska, P. V. McClintock, M. Paluš, J. Petrovčič, S. Ribarič, F. F. Bajrović, J. of Physiology 580 (2007) 315–326. doi:10.1113/jphysiol.2006.126748.

[40] W. Liu, B. Tang, Expert Syst. Appl. 38 (2011) 7575 – 7581. doi:10.1016/j.eswa.2010.12.107.

[41] P. Kvandal, L. Sheppard, S. A. Landsverk, A. Stefanovska, K. A. Kirkeboen, J. Clin. Monit. Comput. 27 (2013) 375–383. doi:10.1007/s10877-013-9484-z.

[42] S. Mallat, A Wavelet Tour of Signal Processing: The Sparse Way, 3 ed., Elsevier Academic Press, Burlington, MA, 2008.

[43] I. Daubechies, Ten Lectures on Wavelets, CBMS-NSF Regional Conference Series in Applied Mathematics, Society for Indus-trial and Applied Mathematics, 1992.

[44] E. O. Doebelin, System Modeling and Response, John Wiley & Sons Inc, 1980.

[45] N. Goodman, The Annals of mathematical statistics 34 (1963) 152–177.

[46] R. J. Baxley, B. T. Walkenhorst, G. Acosta-Marum, in: Global Telecommunications Conference (GLOBECOM 2010), 2010 IEEE, pp. 1–5.

[47] M. K. Simon, Probability Distributions Involving Gaussian Ran-dom Variables, Springer Science, New York, 2006.

[48] P. O. Amblard, M. Gaeta, J. L. Lacoume, Signal Proc. 53 (1996) 1–13.

[49] M. Priestley, Spectral Analyses and Time Series, Academic Press, London, 1981.